

Dispersion of a passive scalar within and above an urban street network

Article

Accepted Version

Goulart, E. V., Coceal, O. and Belcher, S. E. (2018)
Dispersion of a passive scalar within and above an urban
street network. *Boundary-Layer Meteorology*, 166 (3). pp. 351-
366. ISSN 0006-8314 doi: <https://doi.org/10.1007/s10546-017-0315-5> Available at <http://centaur.reading.ac.uk/72996/>

It is advisable to refer to the publisher's version if you intend to cite from the work. See [Guidance on citing](#).

To link to this article DOI: <http://dx.doi.org/10.1007/s10546-017-0315-5>

Publisher: Springer

All outputs in CentAUR are protected by Intellectual Property Rights law, including copyright law. Copyright and IPR is retained by the creators or other copyright holders. Terms and conditions for use of this material are defined in the [End User Agreement](#).

www.reading.ac.uk/centaur

CentAUR

Central Archive at the University of Reading

Reading's research outputs online

1 **Dispersion of a passive scalar within and above an**
2 **urban street network**

3 **EV Goulart · O Coceal · SE Belcher**

4
5 Received: DD Month YEAR / Accepted: DD Month YEAR

6 **Abstract** The transport of a passive scalar from a continuous point-source
7 release in an urban street network is studied using direct numerical simulation
8 (DNS). Dispersion through the network is characterized by evaluating
9 horizontal fluxes of scalar within and above the urban canopy and vertical ex-
10 change fluxes through the canopy top. The relative magnitude and balance of
11 these fluxes are used to distinguish three different regions relative to the source
12 location: a near-field region, a transition region and a far-field region. The par-
13 titioning of each of these fluxes into mean and turbulent parts is computed.
14 It is shown that within the canopy the horizontal turbulent flux in the street
15 network is small, whereas above the canopy it comprises a significant fraction
16 of the total flux. Vertical fluxes through the array top are predominantly tur-
17 bulent. The mean and turbulent fluxes are respectively parametrized in terms
18 of an advection velocity and a detrainment velocity and the parametrization
19 incorporated into a simple box-network model. The model treats the coupled
20 dispersion problem within and above the street network in a unified way and
21 predictions of mean concentrations compare well with the DNS data. This
22 demonstrates the usefulness of the box-network approach for process studies
23 and interpretation of results from more detailed numerical simulations.

EV Goulart
Department of Meteorology, University of Reading, PO Box 243, Reading, RG6 6BB, UK
Tel.: +55-27-40092177
Fax: +55-27-40092148
E-mail: elisa.goulart@ufes.br
Present address: Federal University of Espirito Santo, Vitoria, Brazil

O Coceal
National Centre for Atmospheric Science (NCAS), Department of Meteorology, University
of Reading, PO Box 243, Reading, RG6 6BB, UK

SE Belcher
Department of Meteorology, University of Reading, PO Box 243, Reading, RG6 6BB, UK

24 **Keywords** Dispersion model · Street network · Urban dispersion

25 1 Introduction

26 Noteworthy studies of dispersion in urban areas include a number of detailed
27 field and scaled model experiments (e.g., Davidson et al., 1995, 1996; Mac-
28 donald et al., 1997, 1998; Yee and Biltoft, 2004; Yee et al., 2006; Hilderman
29 et al., 2007; Carpentieri et al., 2009) as well as high-resolution numerical sim-
30 ulations (e.g., Hanna et al., 2002; Milliez and Carissimo, 2007; Branford et al.,
31 2011; Philips et al., 2013). These have provided insight into how the presence
32 of buildings modifies concentration levels in urban areas and what flow and
33 dispersion processes contribute to these differences. For a general context, we
34 refer the reader to reviews included in Britter and Hanna (2003) and Branford
35 et al. (2011). Against the apparent complexity of empirical results, it is helpful
36 to ask whether a core set of robust dispersion processes can be identified that
37 could be of practical use in building approaches to model dispersion in the
38 urban environment.

39 The need for urban dispersion models suitable for operational air-quality
40 and emergency-response applications in particular requires novel approaches
41 that can represent potentially complex turbulent flow processes in a simpli-
42 fied way. Recently Belcher et al. (2015) have proposed a simple approach for
43 modelling dispersion in a *street network regime*, where the buildings are close
44 enough that a distinct network of streets emerges. The methodology follows
45 Soulhac (2000) who developed the governing equations for a family of network
46 models, together with methods for estimating the model parameters, which
47 then led to the development of an operational dispersion model, SIRANE
48 (Soulhac et al., 2011, 2012, 2016). Hamlyn et al. (2007) constructed a much
49 simpler network model for dispersion through an array of cubes, showing im-
50 pressive agreement with measurements made in a water channel by Hilderman
51 et al. (2007). Belcher (2005) and Belcher et al. (2015) developed an analytical
52 model for the dispersion of a passive scalar within a regular street network,
53 which showed that the concentration is given in a closed form solution that
54 includes an explicit dependence on the basic geometrical and flow parameters,
55 which combine into only three effective parameters. Despite the important the-
56 oretical insight that this solution provides, the authors found that the solution
57 is restricted to the so-called near-field regime, where the vertical dispersion is
58 dominated by detrainment out of the street network into the flow above. Be-
59 yond the near-field region the re-entrainment of material back into the street
60 network needs to be taken into account; this cannot be handled analytically in
61 a robust way, although Belcher et al. (2015) gained additional insight through
62 the use of a toy model for re-entrainment. Moreover, the dispersion above the
63 canopy must be modelled too, as the interaction between the canopy and the
64 flow above is a two-way process.

65 Against this background, our study is motivated by the aim of developing
66 a simple model based on a minimal set of processes that will produce reli-

able estimates of the mean concentration both in the near-field region and beyond. The requirement of simplicity stems from the need for viable approaches for modelling in emergency-response or regulatory contexts. The interest in a process-based approach ensures that the very design of the model rests upon sound physical insights. This requires that we have an understanding of which processes are the most important to include and how best to parametrize them. The objectives are therefore two-fold: (i) In order to better understand the dispersion processes both within and above the urban canopy and how they interact we propose to analyze data from a previously-performed direct numerical simulation (DNS) over an array of cubical buildings (Branford et al., 2011). (ii) We extend the model of Belcher et al. (2015) to treat the dispersion both within and above the street network in a coupled way; this then explicitly represents the re-entrainment of material into the street network beyond the near-field regime.

The paper is structured as follows: Sect. 2 outlines the DNS dataset and method of analysis adopted; Sect. 3 is devoted to reporting and discussing results from analysis of the DNS data on the horizontal and vertical transport within and above the street network. In Sect. 4 the main results are used to formulate a simple street network model and to perform numerical experiments and parameter sensitivity studies with it. Conclusions are given in Sect. 5.

2 Numerical data and analysis

This section briefly outlines the DNS dataset and the method of analyzing the data.

2.1 Direct numerical simulations over a regular array

DNS data of Branford et al. (2011) are used here. The DNS models the dispersion of passive scalars by numerically solving the scalar equation,

$$\frac{\partial c}{\partial t} + \mathbf{u} \cdot \nabla c = D \nabla^2 c + S, \quad (1)$$

where c is the concentration of scalar, \mathbf{u} is the instantaneous velocity field vector, D is the molecular diffusivity and S is a source term. The instantaneous turbulent velocity field \mathbf{u} is a solution of the Navier-Stokes equations. The Schmidt number $Sc \equiv \nu/D = 1$ in all the simulations. A steady point-source release near the ground was simulated, so that the source term is given by $S = q \delta^3(\mathbf{x} - \mathbf{x}_s)$, where q is a constant source emission rate, \mathbf{x} is the position vector, \mathbf{x}_s is the position vector of the source and $\delta^3(\mathbf{x})$ is the Dirac delta function. In practice, the source is discretized as a Gaussian ball over a few grid points. The computational set-up, consisting of a regular array of cubes, allowed for multiple independent scalar fields to be modelled during each simulation. Figure 1a shows the computational domain and source locations, with

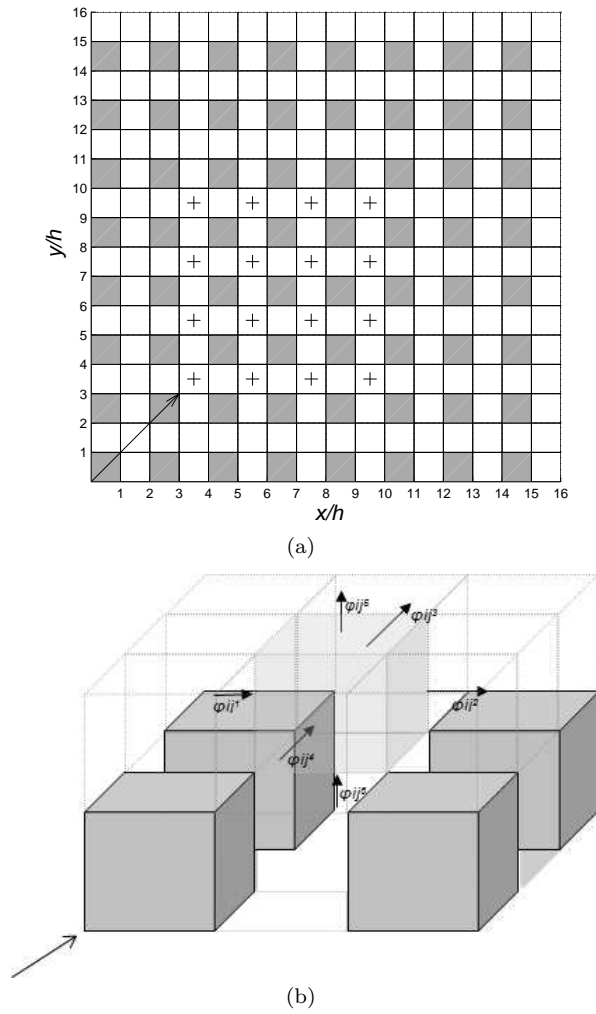


Fig. 1 (a) Plan view of the computational domain in the DNS. Plus signs denote locations of the ground sources. (b) Schematic of fluxes through a box above an intersection.

102 a mean flow direction of 45° as indicated in the figure. We note that the flow
 103 is symmetric with respect to the two horizontal components, u and v . Much
 104 existing work in the literature has dealt with cases where the mean flow is
 105 either aligned with or perpendicular to streets. However, these idealised cases
 106 almost never occur under actual meteorological conditions; indeed they give
 107 rise to somewhat artificial flow regimes. A mean flow oblique to the streets
 108 constitutes a more realistic scenario.

109 The DNS employed dimensionless units, with lengths normalised by the
 110 building height h , velocities normalised by the friction velocity u_τ and with the

111 density of air $\rho = 1$. All quantities and parameters are given in corresponding
 112 dimensionless units unless otherwise stated.

113 Time- and ensemble- averaged concentration statistics showed very good
 114 agreement with experimental data (Branford et al., 2011). The data generated
 115 from these simulations are here analyzed within a box-network framework,
 116 described in the next section.

117 2.2 Analysis within a box-network framework

118 In the box-network framework an array of buildings is considered as forming
 119 a network of ‘streets’ (here defined as the space between adjacent buildings)
 120 joined at ‘intersections’; each of the streets and intersections can be thought of
 121 as a box, through whose facets a scalar can enter or leave. Goulart et al. (2016)
 122 showed that to a first approximation the scalar is generally well mixed in each
 123 such box except near the source and the edges of the plume. Further layers of
 124 boxes can be envisaged above the streets, intersections and buildings as shown
 125 in Fig. 1b. The transport of scalars in such a street network can be analyzed
 126 by considering the fluxes entering and leaving the boxes. Such an approach
 127 forms the basis of a family of street network dispersion models (Soulhac, 2000;
 128 Belcher, 2005; Hamlyn et al., 2007; Soulhac et al., 2011; Belcher et al., 2015),
 129 a version of which will be presented in Sect. 4. To inform the development of
 130 such a model, in Sect. 3 scalar fluxes over the facets of the boxes are computed
 131 from the DNS data.

132 3 Scalar transport through a street network: results from DNS

133 Dispersion of scalars through the street network is controlled by horizontal
 134 fluxes within and above the urban canopy and by vertical exchange fluxes
 135 through the canopy top linking these two regions. Each of these fluxes can be
 136 formally decomposed into a mean and a turbulent component,

$$\langle \overline{cu_i} \rangle = \langle \bar{c} \bar{u}_i \rangle + \langle \overline{c' u_i'} \rangle, \quad (2)$$

137 where c is the instantaneous concentration and u_i is an instantaneous velocity
 138 component perpendicular to the relevant facet. In Eq. 2 the overbar denotes
 139 time-averaging and angled brackets denote spatial averaging over a facet. Hor-
 140 izontal and vertical fluxes within and above the array and their mean and
 141 turbulent components are computed from the DNS data. The results are then
 142 applied in the configuration of the network model in Sect. 4.

143 3.1 Horizontal scalar fluxes within and above the canopy

144 Horizontal scalar fluxes within the canopy calculated from the DNS data are
 145 plotted as a fraction of the total flux at different locations from the source in

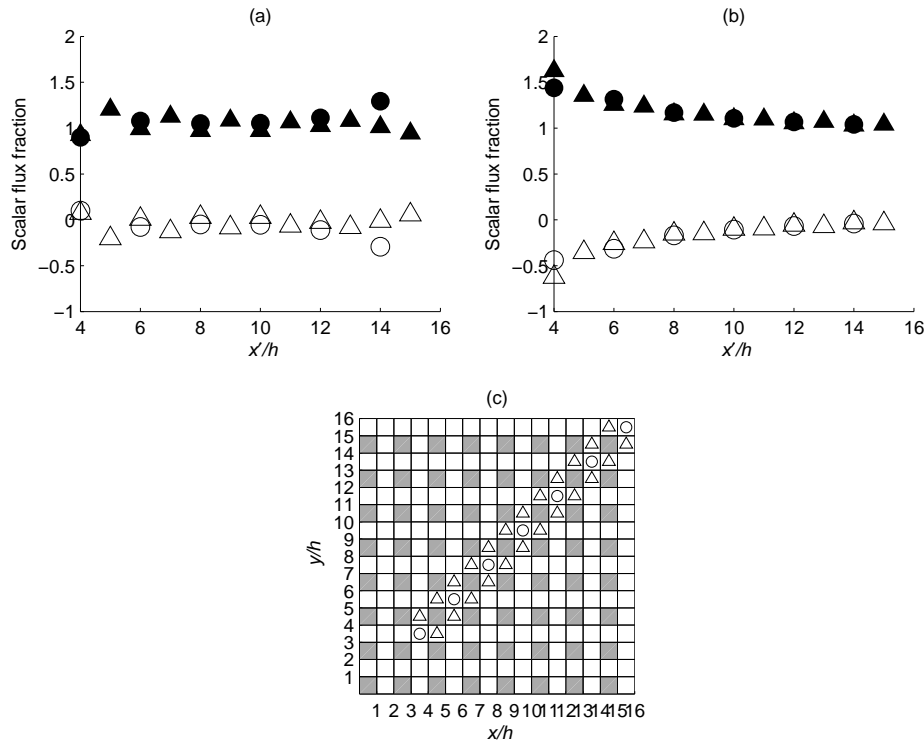


Fig. 2 Ratio of horizontal scalar fluxes, (a) within the canopy, (b) above the canopy. Filled symbols: ratio of mean to total flux $\langle \bar{c} \bar{u} \rangle / \langle \bar{c} \bar{u} \rangle$. Empty symbols: ratio of turbulent to total flux $\langle \bar{c}' \bar{u}' \rangle / \langle \bar{c} \bar{u} \rangle$. (c) Sampling locations. Circles: intersections. Triangles: streets. x' represents the spanwise direction.

146 Fig. 2a. The locations of the boxes in which the fluxes were calculated lie along
 147 three transects, as shown in Fig. 2c. We note that the middle transect involves
 148 only intersections and the other two transects involve only streets. The results
 149 for the latter two transects have been averaged. It is apparent from Fig. 2a
 150 that, for both streets and intersections, the mean flux is much larger than the
 151 turbulent flux irrespective of distance from the source. The average value of
 152 the ratio of mean to total vertical flux in the canopy is $\langle \bar{c} \bar{u} \rangle / \langle \bar{c} \bar{u} \rangle = 0.99$ (and
 153 similarly for the v components, by symmetry). This ratio is relatively constant
 154 throughout the array.

155 Figure 2b shows flux fractions along corresponding transects for the layer
 156 of boxes just above the buildings. The most noteworthy difference is that the
 157 turbulent fluxes are now negative and comprise a significant fraction of the
 158 total flux (up to 0.5). The mean flux fraction is always larger than 1, with a
 159 maximum value of about 1.5. The average value of the ratio of mean to total
 160 vertical flux just above the canopy is $\langle \bar{c} \bar{u} \rangle / \langle \bar{c} \bar{u} \rangle = 1.27$. The corresponding
 161 average turbulent flux ratio is therefore $\langle \bar{c}' \bar{u}' \rangle / \langle \bar{c} \bar{u} \rangle = -0.27$. The occurrence

162 of this large counter-gradient turbulent flux ratio above the canopy contrasts
 163 with the small positive value of 0.01 within the canopy. The origin of these
 164 negative turbulent fluxes is unclear; a possible mechanism could involve ejections
 165 associated with coherent structures above the canopy (e.g., Coceal et al.,
 166 2007).

167 3.2 Vertical scalar fluxes through the canopy top

168 The mean and turbulent components of the vertical flux through the top of
 169 the array are shown in Fig. 3. The mean vertical flux $\langle \bar{c} \bar{w} \rangle$ is always positive in
 170 the intersections and always negative in the streets (Fig. 3a). Since \bar{c} is always
 171 positive, the sign of $\langle \bar{c} \bar{w} \rangle$ is determined by that of \bar{w} . Hence, the pattern of
 172 mean inflow or outflow is determined by the mean vertical velocity pattern.
 173 The vertical velocity averaged over the top facet of a street $\langle \bar{w} \rangle$ is indeed
 174 downward, whereas it is upward over an intersection (not shown). We note
 175 that the mean vertical flux from the first intersection (which contains the
 176 source) is anomalously low; see below.

177 There is little difference between the turbulent fluxes $\langle c'w' \rangle$ for streets and
 178 intersections (Fig. 3b). They are positive for both streets and intersections in
 179 the near-field region, but becomes slightly negative from the third intersection
 180 onwards. The maximum turbulent flux is about an order of magnitude larger
 181 than the maximum mean flux. The turbulent flux decays much quicker with
 182 distance from the source than the mean vertical flux. This may be because
 183 turbulent scalar exchanges take place in both directions, and hence tend to
 184 equalise quicker.

185 The ratios of the mean and turbulent vertical fluxes to the total vertical
 186 flux (Fig. 3c) reveal the following: (i) Up to a distance of about four building
 187 heights from the source the turbulent flux is the dominant component for
 188 both streets and intersections. (ii) However, far from the source (beyond a
 189 distance of about ten building heights) there is considerable scatter in the flux
 190 ratio. This is because both the turbulent and mean fluxes are small in the
 191 far-field region. The turbulent flux is slightly negative for intersections and
 192 both turbulent and mean flux are negative for streets.

193 3.3 Horizontal vs. vertical transport

194 The vertical flux through the canopy top exerts a strong control on how a
 195 plume spreads through a street network. Vertical detrainment from the canopy
 196 results in a reduction in the amount of material available to disperse horizon-
 197 tally through the canopy; this should cause a rapid fall-off of the concentration
 198 with distance from the source. However, material can also be re-entrained into
 199 the canopy further downstream. The balance between detrainment and re-
 200 entrainment is not the only factor that determines the subsequent horizontal
 201 fall-off. Equally important is the lateral spread through the canopy.

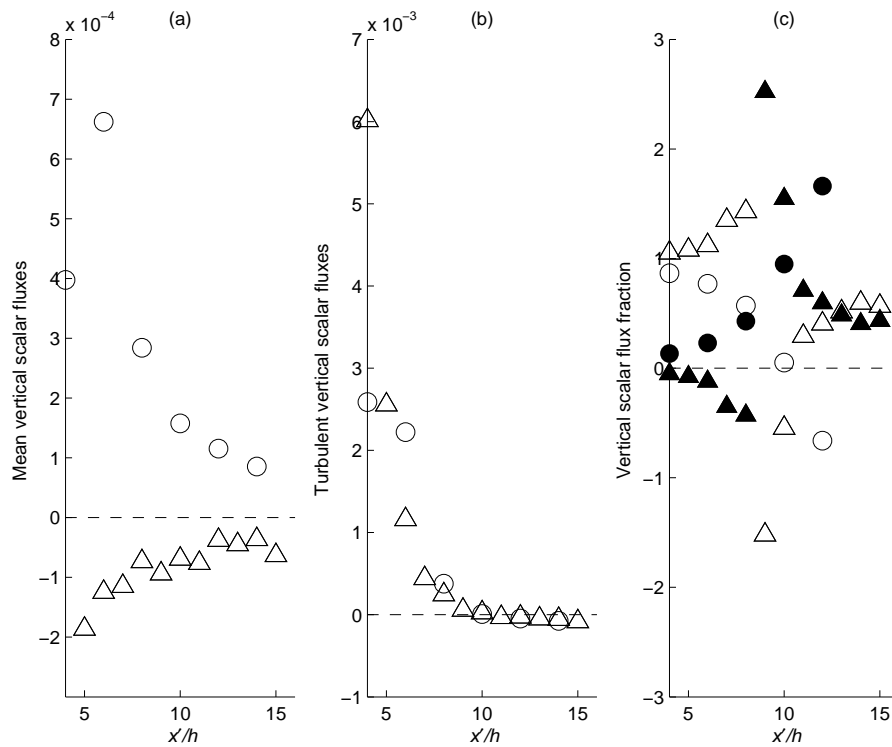


Fig. 3 Vertical fluxes through the canopy top at the same sampling locations as in 2c. (a) mean, (b) turbulent, (c) ratio of mean (filled symbols) and turbulent (empty symbols) to total. Circles: intersections. Triangles: streets. Fluxes have been normalized using the release rate q .

202 Figures 4a, 4b and 4c respectively show the horizontal scalar flux through
 203 the canopy, vertical flux through the canopy top, and the ratio of vertical to
 204 horizontal flux, as a function of distance from the source. There is a rapid
 205 decrease in both the horizontal and vertical fluxes up to the third intersection
 206 downstream, followed by a much more gradual decrease thereafter. The total
 207 horizontal flux behaves in roughly the same way in streets and intersections.
 208 In contrast, there is a clear difference between the vertical fluxes in the streets
 209 and the intersections; the near-field and far-field behaviours also differ. The
 210 vertical flux in the intersections is generally positive, so that material is nearly
 211 always detrained out of the intersections into the air above. The vertical flux
 212 in the streets is positive close to the source but changes sign between the
 213 second and third intersections downstream. This implies that re-entrainment
 214 begins to exceed detrainment very rapidly downstream of the release, at least
 215 in the present set-up. The magnitude of the flux in the intersections is larger
 216 than that from the streets in the near-field region (up to the third intersection
 217 downstream of the release). As noted earlier, the vertical flux in the first
 218 intersection (which contains the source) is anomalously low compared to that

219 in the streets immediately adjacent to it. This arises because material released
220 in an intersection is rapidly swept to the next streets downstream, caught in the
221 wakes of adjacent buildings and pushed upwards by a strong updraft (Coceal
222 et al., 2014). This gives rise to ‘secondary wake sources’ (Vincent, 1978) in
223 the relevant streets, which detrain material at a much higher rate than in the
224 intersection where the source is located. Secondary sources were also observed
225 in previous experimental studies, e.g. Davidson et al. (1995, 1996).

226 Fig. 4c shows that the magnitude of the vertical flux is generally less than a
227 quarter of the horizontal flux, except at the location furthest from the source
228 (where both fluxes are small). After an initial increase with distance from
229 the source location this ratio decreases steadily up to the third intersection.
230 Beyond this point there is a difference in the behaviour in intersections and
231 streets. In intersections there is a continual slow decrease towards zero. In
232 streets the ratio becomes negative because the vertical flux changes sign due
233 to re-entrainment into the canopy.

234 It is instructive to decompose the vertical flux into an upward component
235 (detrained flux) and a downward component (entrained flux). Figure 4d shows
236 the ratio of the downward flux to the upward flux for the same intersections
237 and streets. The downward flux is a small fraction (around 0.05) of the upward
238 flux in the first intersection after the release location. This fraction then rises
239 nearly linearly to a value of over 0.8 over the next three intersections. In
240 the streets the downward flux comprises a larger fraction of the upward flux,
241 starting at around 0.5 in the first street downwind of the release to over 2 over
242 the next six streets.

243 Based on these observations, it is possible to identify three different regimes
244 based on distance downwind of the source. Very close to the source, the vertical
245 upward flux is a substantial fraction (up to around 0.25) of the horizontal flux
246 through the network. In the intermediate region the vertical flux consists of
247 both an upward and a downward component of comparable magnitudes, so
248 that the net vertical flux is a smaller fraction of the horizontal flux. Further
249 downwind, there is a qualitative difference in the behaviour in streets and
250 intersections. In intersections the ratio of downward to upward flux approaches
251 (but does not exceed) 1; hence the ratio of the net vertical flux to the horizontal
252 flux approaches 0. In streets the downward flux exceeds the upward flux and
253 hence the net vertical flux becomes negative; it is a non-negligible fraction
254 (around 0.15) of the horizontal flux. However, these differences are probably
255 unimportant since the vertical fluxes are very small and the concentrations
256 within the canopy and above are virtually the same at this distance. Indeed,
257 the plume is vertically well-mixed both through the canopy and immediately
258 above it beyond the third intersection from the source (Fig. 5).

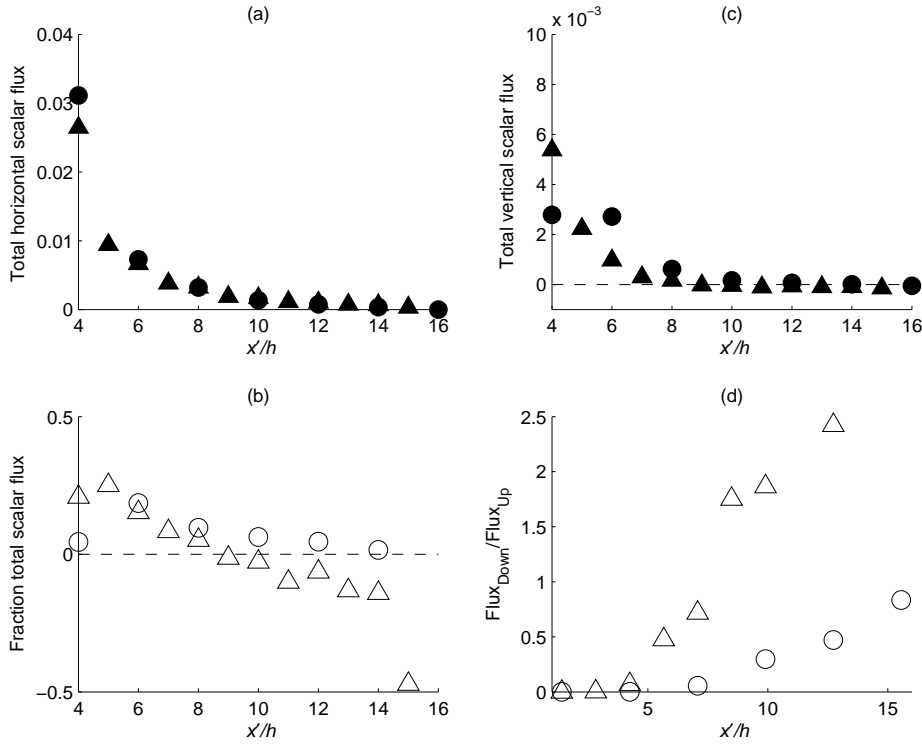


Fig. 4 Comparison between horizontal fluxes through the canopy and vertical fluxes out of the canopy top: (a) total horizontal flux, (b) total vertical flux, (c) ratio of vertical to horizontal flux, (d) ratio of downward flux to upward flux. Fluxes have been normalised using the release rate q .

259 **4 A process-based model of dispersion within and above a street** 260 **network**

261 The results of the last section motivate an approach for modelling dispersion
262 through a network of streets by considering the balance of fluxes through a coupled
263 system of boxes representing each street and intersection in the network.
264 This approach forms the basis of the SIRANE model (Soulhac, 2000; Soulhac
265 et al., 2011, 2012), used operationally for air quality modelling. Belcher
266 et al. (2015) recently developed an analytical model for regular street net-
267 works, which demonstrated how the geometrical and flow parameters combine
268 into a small number of non-dimensional effective parameters that control the
269 dispersion in the network. We now generalize the analytical model developed
270 by Belcher et al. (2015) to include dispersion above the street network. The
271 resulting equations cannot be solved analytically, but can be readily modelled
272 numerically. Our aim here is to develop a minimal model that is as simple as
273 possible while still capturing the most important processes identified from the
274 analysis presented in Sect. 3. In doing so we do not claim that the assump-

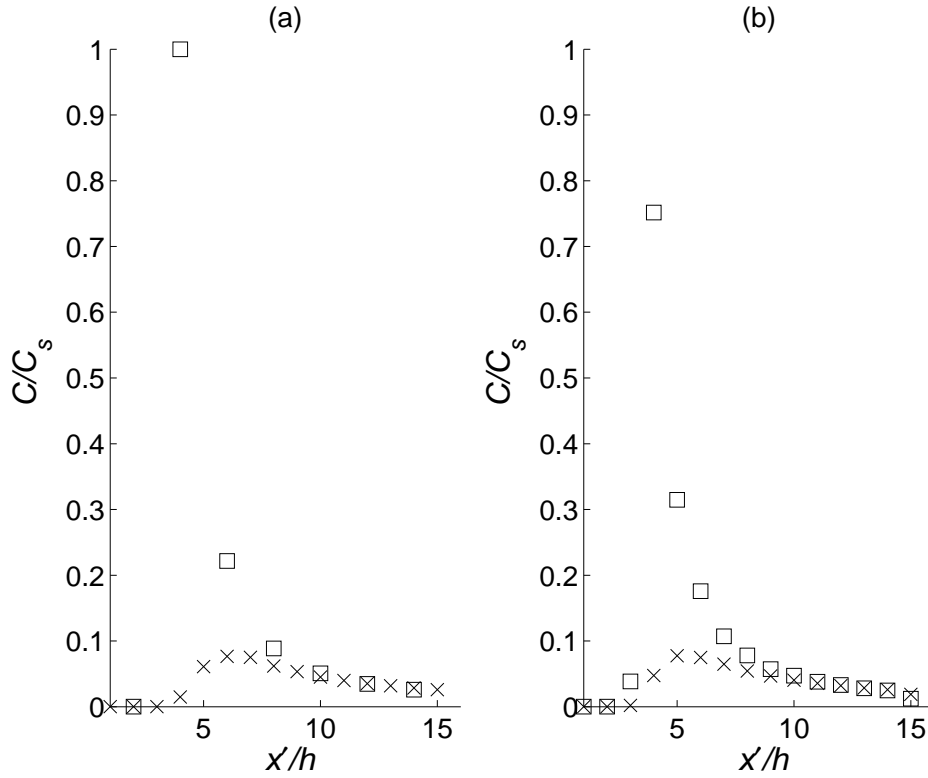


Fig. 5 Variation of mean concentration with distance from the source, (a) intersections, (b) streets. Squares: within canopy. Crosses: above canopy. The concentration is normalized by the concentration in the source box, C_s

275 tions made here have complete generality; indeed some of them will need to
 276 be modified in other contexts.

277 4.1 Governing equations

Following a rigorous formalism (Belcher et al., 2015), we represent each street and intersection as a box and take the volume- and ensemble-average of the scalar conservation equation over the volume V of the box to give

$$\frac{dC}{dt} + \frac{1}{V} \int_{\partial V} \overline{c\mathbf{u}} \cdot d\mathbf{S} = Q, \quad (3)$$

278 where C and Q are the ensemble- and volume-averaged concentration and
 279 source emission rate in the box, ∂V is the surface area enclosing the box, and
 280 the overline denotes an ensemble average.

The flux term can be separated into mean and turbulent scalar fluxes,

$$\int_{\partial V} \bar{c}\bar{\mathbf{u}} \cdot d\mathbf{S} = \int_{\partial V} \bar{c}\bar{\mathbf{u}} \cdot d\mathbf{S} + \int_{\partial V} \overline{c'\mathbf{u}'} \cdot d\mathbf{S}, \quad (4)$$

where primes denote fluctuations from the ensemble average. The mean and turbulent fluxes are each parametrized as described in the next section.

4.2 Parametrization of the fluxes

Belcher et al. (2015) show that the mean flux density $\bar{c}\bar{\mathbf{u}}$ can be written formally as the product $\langle \bar{\mathbf{u}} \rangle_{\partial V}$ of the velocity averaged over the area ∂V and an average concentration C_a ,

$$\bar{c}\bar{\mathbf{u}} = C_a \langle \bar{\mathbf{u}} \rangle_{\partial V}. \quad (5)$$

In the next section, the facet-averaged mean velocity is computed from the DNS data. The formally undetermined average concentration C_a can be approximated as the volume-average concentration in each box, assuming that the scalar is well-mixed. Goulart (2012) and Belcher et al. (2015) demonstrate that this is a reasonable approximation for the current set-up.

Following Belcher et al. (2015), the turbulent flux density is parametrized assuming the gradient diffusion model,

$$\overline{c'\mathbf{u}'} = -\mathbf{K}\nabla\bar{c}, \quad (6)$$

where $\mathbf{K} = \text{diag}(K_x, K_y, K_z)$ is a diagonal matrix with diagonal components equal to the eddy diffusivity coefficients K_x, K_y and K_z in the x, y and z directions respectively.

It is common to represent the scalar exchange between the canopy and the air above with a detrainment velocity E , defined as

$$E = \frac{K_z}{\Delta z}, \quad (7)$$

where Δz is an appropriate vertical distance, here taken to be the vertical separation between the centres of a box in the canopy and the one immediately above it.

We can generally neglect the horizontal turbulent flux within the canopy, except when the flow direction is closely aligned with one of the streets. Additionally, the mean vertical flux can be neglected in comparison with the turbulent vertical flux.

It is straightforward to discretize Eq. 3. A first-order scheme yields the following, for each box

$$\Delta C = \frac{\Delta t}{V} \left(\sum_{k=1}^n F^k + \sum_{k=1}^n f^k + Q \right), \quad (8)$$

where F^k and f^k are respectively the advective and diffusive scalar fluxes through each facet k of the box and n is the total number of facets enclosing the box.

305 4.3 Calculation of model parameters from DNS

306 For the current DNS set-up, with the flow at 45° to the regular cubical array,
 307 the horizontal facet-averaged advection velocity components $\langle \bar{u} \rangle_k$ and $\langle \bar{v} \rangle_k$ are
 308 approximately equal. Figure 6a shows the average of $\langle \bar{u} \rangle_k$ and $\langle \bar{v} \rangle_k$ computed
 309 for intersections and streets along the transects shown in Fig. 2c. The advection
 310 velocities in intersections (average value 1.13) are slightly lower than in streets
 311 (average value 1.18). The facet-averaged velocities in the boxes just above the
 312 array (around 3.4) are about three times those in the array (not shown). For
 313 comparison, Fig. 6a also shows corresponding values of ‘flux velocities’, defined
 314 as the ratio of $\overline{c\mathbf{u}}$ and C_a . There is a difference of around 10 – 15% between
 315 the facet-averaged velocities and the flux velocities. This gives an indication of
 316 the margin of error involved in using the facet velocity as an input parameter
 317 in the model.

The detrainment velocity E characterizing vertical turbulent transfer out
 of the canopy top is computed as follows:

$$E = \frac{\langle c'w' \rangle}{(C_{in} - C_{abv})}, \quad (9)$$

318 where C_{in} and C_{abv} are the box-averaged mean concentration within and above
 319 the canopy respectively, and the facet average of the vertical flux (indicated
 320 by the angled brackets) is taken over the interface separating the two boxes.

321 Figure 6b shows the detrainment velocity at the same locations in streets
 322 and intersections as in Fig. 6a. Values are plotted only up to a distance of $8h$
 323 from the source since both the vertical flux and concentration difference be-
 324 come tiny beyond this distance, giving indeterminate values for their ratio. The
 325 difference in detrainment velocity in streets and intersections is evident. In-
 326 tersections have, on average, a detrainment velocity approximately 60% larger
 327 than streets. The average detrainment velocity for streets and intersections
 328 are: $E_s = 0.3$ and $E_i = 0.5$.

329 Values for the diffusion coefficients K_x , K_y and K_z can be computed from
 330 the DNS data, with $K_x = K_y = 0.5$ and $K_z = 0.3$ used here. These values are
 331 consistent with those used in the literature for rough surfaces (e.g. Pasquill,
 332 1962).

333 5 Numerical experiments with the network model

334 The parameters calculated from the DNS data in the last section are summa-
 335 rized in Table 1. These values are used as input to configure a set of runs with
 336 the network model described in Sect. 4.

337 Figure 7 shows comparisons between the mean concentrations computed by
 338 the network model (indicated by triangles) and the DNS (indicated by circles)
 339 along the plume centreline and along lateral transects at different distances
 340 from the source. The network model generally captures well both the decay

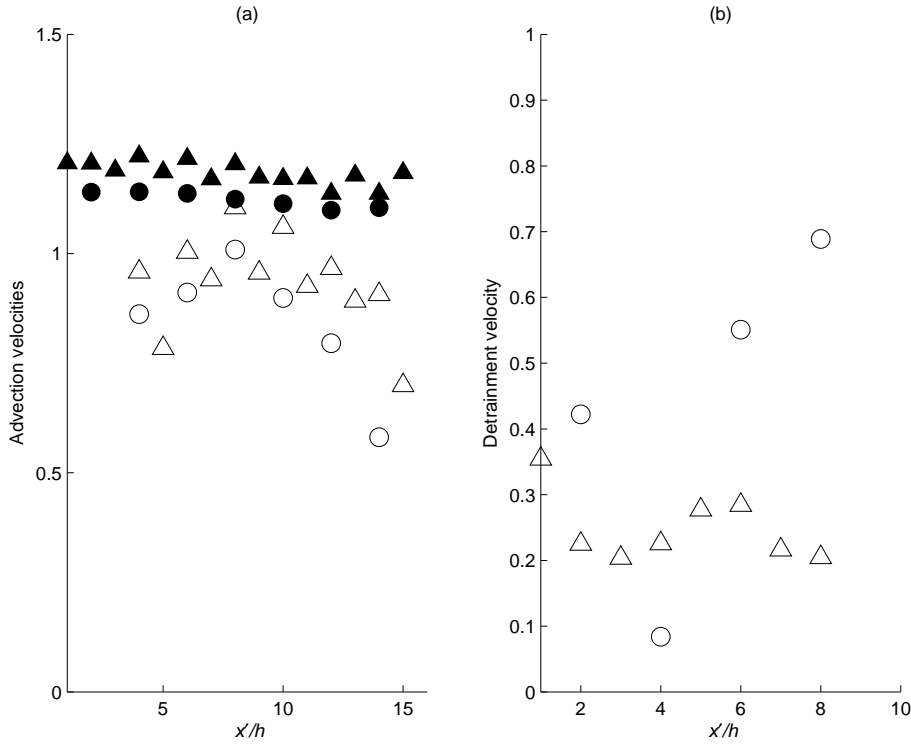


Fig. 6 (a) Filled symbols: facet-averaged advection velocities within the canopy. Empty symbols: flux advection velocity. (b) Detrainment velocities. Circles: intersections. Triangles: streets. Locations correspond to Fig. 2c.

$U_i \approx V_i$	$U_s \approx V_s$	E_i	E_s	$U_{abv} \approx V_{abv}$	K_x	K_y	K_z
1.13	1.18	0.5	0.3	3.43	0.5	0.5	0.3

Table 1 Non-dimensional input parameters for the network model. Here U and V denote horizontal facet-averaged velocity components in the x and y directions respectively. The subscripts i and s refer to intersections and streets respectively, while abv refers to the layer just above the canopy layer.

341 in the centreline concentration and the lateral spread of the plume. The values
 342 predicted by the network model are generally within around 30% of the
 343 DNS values. This is encouraging, given the extreme simplicity of the model
 344 compared to the DNS.

345 Corresponding profiles in the layer just above the canopy are shown in
 346 Fig. 8. The agreement with the DNS is even better than in the canopy. It
 347 is especially good further from the source, from a distance of around $6h\sqrt{2}$
 348 onwards. Close to the source, at a distance of $2h\sqrt{2}$, the model underpredicts
 349 the concentration above the canopy by up to around 30%. This is consistent
 350 with an overprediction within the canopy by approximately the same amount.
 351 This is likely a result of secondary wake sources in the streets close to the

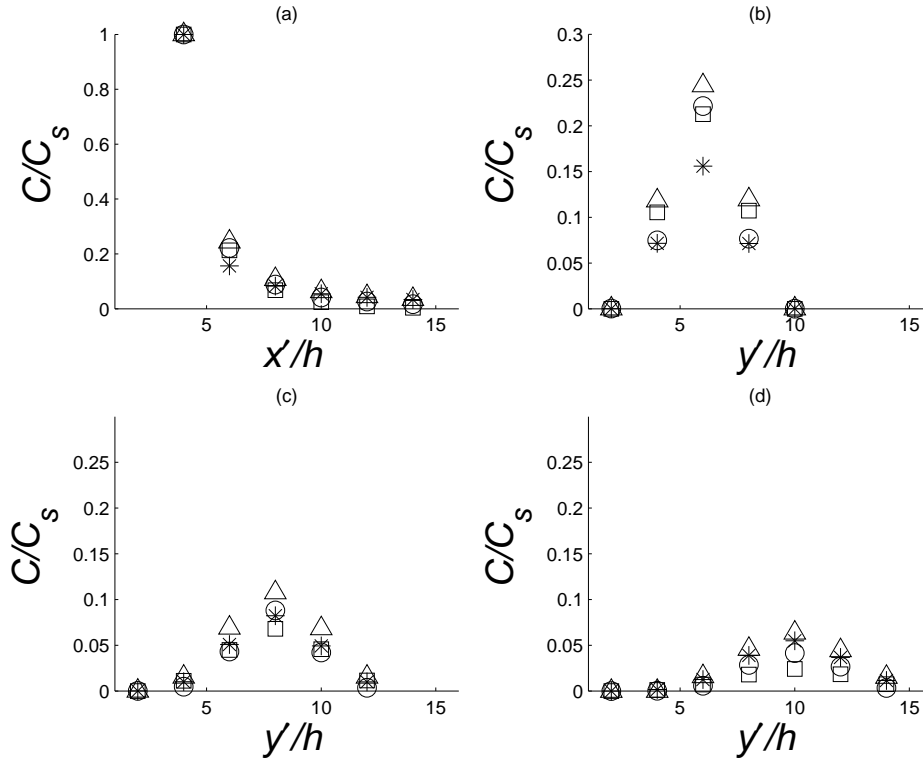


Fig. 7 Comparison between in-canopy concentration computed from network model and DNS (a) Centreline. Lateral profiles at (b) $2h\sqrt{2}$, (c) $4h\sqrt{2}$ and (d) $6h\sqrt{2}$ from the source. Triangles: network model without secondary sources. Asterisks: network model with secondary sources. Squares: analytical solution of Belcher et al. (2015). Circles: DNS. Distances along and perpendicular to the plume centreline are denoted by x' and y' respectively.

352 release, which lead to an enhanced initial detrainment of material (Coccal et
 353 al. 2014). The network model does not represent these secondary sources.

354 A crude way to investigate the possible effect of the secondary sources is
 355 to simply increase the detrainment velocity in the relevant streets where they
 356 occur. The star symbols in Figs. 7 and 8 show the effect of increasing E_s to 2,
 357 which is approximately 6.7 times the value in other streets. This indeed leads to
 358 closer correspondence with the DNS near the source, while the values further
 359 away are much less affected. This shows that any enhanced initial detrainment
 360 due to the secondary sources is compensated by greater re-entrainment further
 361 afield.

362 The sensitivity of the predicted concentrations to the input parameters is
 363 investigated by increasing and decreasing each parameter independently by
 364 10%. The concentration is then averaged along the plume centreline over six
 365 successive intersections, including the intersection in which the source is lo-
 366 cated. The averaged concentration along a lateral transect at a distance of

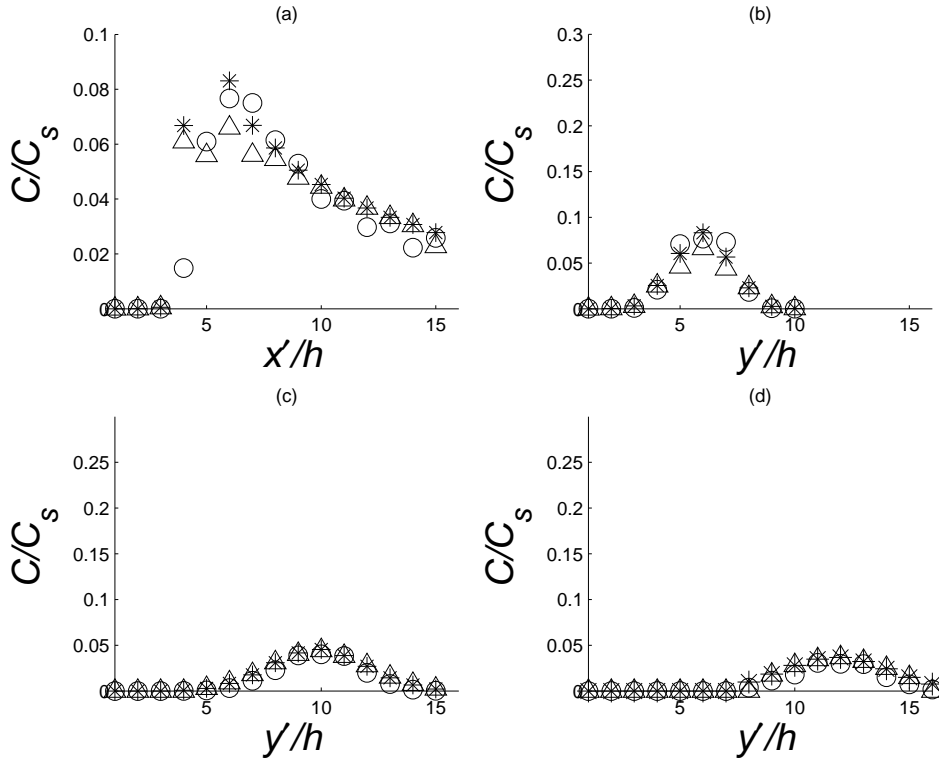


Fig. 8 Comparison between above-canopy concentration computed from network model and DNS. (a) Centreline. Lateral profiles at (b) $2h\sqrt{2}$, (c) $6h\sqrt{2}$ and (d) $8h\sqrt{2}$ from the source. Triangles: network model without secondary sources. Asterisks: network model with secondary sources. Circles: DNS. x' and y' are the streamwise and spanwise distance to the plume centreline, respectively.

367 $8h$ from the source is also computed. Similar computations are made for cor-
 368 responding boxes just above the canopy layer. Table 2 shows the percentage
 369 difference in the computed concentrations relative to the run performed with
 370 the original input parameter values (as given in Table 1). The results show
 371 that changing the parameters have different effects on the concentration aver-
 372 aged along the centreline, and along the lateral transect. The effect on the
 373 concentration below and above the canopy are also different. On the whole
 374 the advection velocities within the canopy have the largest effect. The above-
 375 canopy concentrations are especially sensitive to the advection velocities in
 376 the intersections, but show little dependence on the advection velocities in the
 377 streets. There is little dependence on the values of K_x and K_y , but a change in
 378 the value of K_z of 10% changes the concentration above the canopy by about
 379 30% on average.

Table 2 Network model sensitivity analysis. $D1$ is the difference between the network model and DNS along the centerline of the plume within the canopy. $D2$ is the difference between the network model and DNS along a lateral profile at $8h\sqrt{2}$ from the source within the canopy. $D3$ is the difference between the network model and DNS along the lateral profile at $9h\sqrt{2}$ from the source above the canopy.

Variables	Increase of 10%			Decrease of 10%		
	D1	D2	D3	D1	D2	D3
U_i, V_i	-7	-12	-40	30	17	211
U_s, V_s	-20	-14	2	39	21	-3
U_{abv}, V_{abv}	13	10	71	-11	-9	-33
E_i	13	7	-13	-12	-7	16
E_s	21	11	0	-16	-10	0
K_x, K_y	1	0	5	-1	0	-5
K_z	5	4	38	-5	-4	-24

380 6 Conclusions

381 The dispersion from a localized source within an idealized street network has
 382 been studied using DNS data. The dispersion characteristics within and above
 383 the network were compared by evaluating horizontal and vertical fluxes and
 384 their partitioning into mean and turbulent parts. The results show that the
 385 horizontal flux within the canopy is almost exclusively comprised of the mean
 386 flux, whereas above the canopy a significant counter-gradient turbulent part
 387 exists. By contrast, the vertical flux through the canopy top is generally dom-
 388 inated by the turbulent component. A fraction of the material originally re-
 389 leased within the canopy and detrained into the air above is re-entrained re-
 390 latively soon downstream. Based on the relative magnitude and balance of
 391 the horizontal and vertical fluxes, three distinct regions have been delineated:
 392 a near-field region, a transition region and a far-field region (summarized in
 393 simplified form in Fig. 9).

394 The results from the DNS have been used to develop a minimal process-
 395 based street network model that treats the dispersion within and above the
 396 network in a unified way. The model incorporates a small set of key urban
 397 dispersion processes including horizontal advection, vertical detrainment and
 398 re-entrainment. A rigorous formulation based on volume-averaging the govern-
 399 ing equations reduced the highly complicated original problem to an effective
 400 model described by only a few parameters. Comparisons with DNS data show
 401 that this highly simplified modelling approach still gives accurate quantitative
 402 estimates of mean concentrations both within and above the street network.
 403 This indicates that the processes included in the model are indeed the most
 404 important ones and that the parametrizations on which it is based are vi-
 405 able. The fact that the input parameters of the simpler model were deduced
 406 from the DNS in the current exercise ensures consistency in the evaluation of
 407 the approach. Naturally, if the model were to be used in a predictive mode,
 408 it would need to be supplemented by methods to determine the parameters
 409 independently.

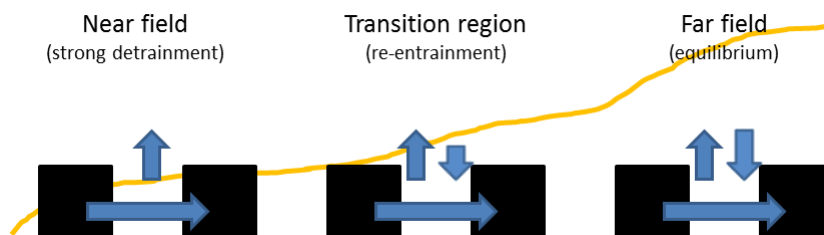


Fig. 9 Plume growth for a ground source release in an urban canopy, with arrows indicating relative magnitudes of horizontal and vertical fluxes in the near-field, the transition and the far-field regions.

410 The method can be readily generalized for other set-ups including non-
 411 regular geometries, although some of the specific assumptions made here may
 412 have to be modified in other scenarios. For example, the operational SIRANE
 413 model (Soulhac et al., 2011, 2012) employs a different model for parametriz-
 414 ing fluxes at intersections that does not assume well-mixed conditions. It also
 415 treats above-roof dispersion as a series of point sources giving rise to Gaus-
 416 sian plumes that are then superimposed. Moreover, as a self-contained opera-
 417 tional model, the SIRANE model includes built-in methods for estimating
 418 the model parameters such as advection and exchange velocities. This work
 419 has focused on examining the conceptual and empirical basis of the under-
 420 lying street-network approach, and to assess its performance when stripped
 421 of as many specific modelling assumptions as possible. One noteworthy result
 422 is that the basic street-network approach, as incorporated in a model much
 423 simpler than even the SIRANE model, shows a promising performance. The
 424 level of agreement obtained with the DNS data shows the predictive potential
 425 of the approach, if used in conjunction with accurate methods of estimating
 426 the model parameters. This implies that efforts to improve the SIRANE model
 427 should focus on further developing and testing such methods.

428 **Acknowledgements** Elisa V. Goulart gratefully acknowledges funding from National Coun-
 429 cil for Scientific and Technological Development (CNPq) and Espirito Santo Research Foun-
 430 dation (FAPES), Brazil. Omduth Coceal gratefully acknowledges funding from the Natural
 431 Environment Research Council (NERC) through their National Centre for Atmospheric
 432 Science (NCAS) under grant no. R8/H12/83/002 and from the Engineering and Physical
 433 Sciences Research Council (EPSRC contract number EP/K040707/1).

434 References

- 435 Belcher S (2005) Mixing and transport in urban areas. *Phil Trans R Soc*
 436 363:2947–2968
 437 Belcher S, Coceal O, Goulart E, Rudd A, Robins A (2015) Processes control-
 438 ling atmospheric dispersion through city centres. *J Fluid Mech* 763:51–81

- 439 Branford S, Coceal O, Thomas T, Belcher S (2011) Dispersion of a point-
440 source release of a passive scalar through an urban-like array for different
441 wind directions. *Boundary-Layer Meteorol* 139:367–394
- 442 Britter R, Hanna S (2003) Flow and dispersion in urban areas. *Annu Rev*
443 *Fluid Mech* 35:469–496
- 444 Carpentieri M, Robins A, Baldi S (2009) Three-dimensional mapping of air
445 flow at an urban canyon intersection. *Boundary-Layer Meteorol* 133:277–296
- 446 Coceal O, Dobre A, Thomas T, Belcher S (2007) Mixing and transport in
447 urban areas. *J Fluid Mech* 589:375–409
- 448 Coceal O, Goulart E, Branford S, Thomas T, Belcher S (2014) Flow structure
449 and near-field dispersion in arrays of building-like obstacles. *J Wind Eng*
450 *Ind Aerodyn* 125:52–68
- 451 Davidson M, Mylne K, Jones C, Phillips J, Perkins R (1995) Plume disper-
452 sion through large groups of obstacles a field investigation. *Atmos Environ*
453 29:3245–3256
- 454 Davidson M, WHSnyder, Lawson R, Hunt J (1996) Wind tunnel simulations of
455 plume dispersion through groups of obstacles. *Atmos Environ* 30:3715–3725
- 456 Goulart E (2012) Flow and dispersion in urban areas. PhD thesis, University
457 of Reading
- 458 Goulart E, Coceal O, Belcher S (2016) Spatial and temporal variability of
459 the concentration field from localized releases in a regular building array.
460 *Boundary-Layer Meteorol* 159:241–257
- 461 Hamlyn D, Hilderman T, Britter R (2007) A simple network approach to mod-
462 elling dispersion among large groups of obstacle. *Atmos Environ* 41:5848–
463 5862
- 464 Hanna S, Tehranian S, Carissimo B, Macdonald R, Lohner R (2002) Compar-
465 isons of model simulations with observations of mean flow and turbulence
466 within simple obstacle arrays. *Atmos Environ* 36:5067–5079
- 467 Hilderman T, Chong R, Kiel D (2007) A laboratory study of momentum
468 and passive scalar transport and diffusion within and above a model ur-
469 ban canopy. Final report Contract Report DRDC Suffield CR 2008-025
- 470 Macdonald R, Griffiths R, Cheah S (1997) Field experiments of dispersion
471 through regular arrays of cubic structures. *Atmos Environ* 31:783–795
- 472 Macdonald R, Griffiths R, Hall D (1998) A comparison of results from scaled
473 field and wind tunnel modelling of dispersion in arrays of obstacles. *Atmos*
474 *Environ* 32:3845–3862
- 475 Milliez M, Carissimo B (2007) Numerical simulations of pollutant dispersion in
476 an idealised urban area, for different meteorological conditions. *Boundary-*
477 *Layer Meteorol* 122:321–342
- 478 Philips D, Rossi R, Iaccarino G (2013) Large-eddy simulation of passive scalar
479 dispersion in an urban-like canopy. *J Fluid Mech* 723:404–428
- 480 Soulhac L (2000) Modelisation de la dispersion atmosferic a l’interieur de la
481 canopee urbaine. PhD thesis, Ecole Centrale de Lyon
- 482 Soulhac L, Salizzoni P, Cierco FX, Perkins R (2011) The model sirane for
483 atmospheric urban pollution dispersion; part i, presentation of the model.
484 *Atmos Environ* 45(39):7379–7395

-
- 485 Soulhac L, PSalizzoni, Mejean P, Didier D, Rios I (2012) The model sirane for
486 atmospheric urban pollutant dispersion; part ii, validation of the model on
487 a real case study. *Atmos Environ* 320-337:49
- 488 Soulhac L, Lamaison G, Cierco FX, Salem NB, Salizzoni P, Mejean P, Armand
489 P, Patryl L (2016) Siranerisk: Modelling dispersion of steady and unsteady
490 pollutant releases in the urban canopy. *Atmos Environ* 140:242-260
- 491 Vincent J (1978) Model experiments on the nature of air pollution transport
492 near buildings. *Atmos Environ* 11:765-774
- 493 Yee E, Biltoft C (2004) Concentration fluctuation measurements in a plume
494 dispersing through a regular array of obstacles. *Boundary-Layer Meteorol*
495 111:363-415
- 496 Yee E, Gailis R, Hill A, Hilderman T, Kiel D (2006) Comparison of wind
497 tunnel and water-channel simulations of plume dispersion through a large
498 array of obstacles with a scaled field experiment. *Boundary-Layer Meteorol*
499 121:389-432